ELSEVIER

A new adaptive remeshing scheme based on the sensitivity analysis of the SPR point wise error estimation

G. Bugeda *

International Center for Numerical Methods in Engineering (CIMNE), Universitat Politècnica de Catalunya (UPC), Escola Universitària d'Enginyers Tècnics Industrials (EUETIB), C/Comte d'Urgell, 187, 08036 Barcelona, Spain

Abstract

This paper presents a formulation for the obtainment of the sensitivity analysis of a point wise error estimator with respect to the nodal coordinates using the adjoint state method. The proposed point wise error estimator is based on the SPR method.

The numerical accuracy of the presented sensitivity analysis has been tested by perturbing a mesh. The capability of the presented sensitivity analysis for the detection of pollution error has also been tested.

A new adaptive remeshing strategy based on the sensitivity analysis of the point wise error estimation has been developed and tested. This strategy produces very cheap meshes for the accurate evaluation of stresses at specific points.
© 2005 Elsevier B.V. All rights reserved.

Keywords: Error estimation; Sensitivity analysis; Adaptivity; Point wise error; Pollution error

1. Introduction

In the solid mechanics context, the idea of improving the mesh quality by using a sensitivity analysis is not new. The first historical reference comes from McNeic and Marcal [1], who proposed to improve a mesh by minimizing the potential energy of the structural problem with respect to the nodal coordinates. This was done by coupling the finite element solution with the mesh sensitivity analysis. Another important reference comes from Kang, Tae and Kwak [2], who maximized the deformation energy with respect to the nodal coordinates. These works allow to optimize a mesh in order to obtain the best solution for a

* Tel.: +34 93 4016494; fax: +34 93 4016517.
E-mail address: bugeda@cimne.upc.edu
URL: http://www.cimne.upc.es/

structural problem with a fixed mesh topology and a fixed number of degrees of freedom. These types of methods are very convenient if the storing capacity and the computational speed are limited. Nevertheless, the increasing power of computers makes the computational power not to be a serious limitation. Due to that, this type of methods is no more in use.

On the other hand, it is possible to obtain specific adaptive remeshing strategies for the control of the point wise error of any physical quantity related with the structural analysis (see Bugeda [3]), but the control of the pollution error (see Babuška [4,5]) obligates to control the local error everywhere, this producing globally adapted meshes with a very high number of degrees of freedom. Nevertheless, when doing a structural analysis we know very often where the points with the highest values of stresses are, and the control of the point wise error not only at those points but everywhere seems to be excessively expensive for just evaluating the stresses at those points.

Furthermore, it is well known (see Babuška [4,5]) that a local refinement around the conflictive points will only minimise the so called ''local error'', but not the ''pollution error''. For this reason, the evaluation of the sensitivity analysis of the point wise error at those points with respect to the nodal coordinates can provide information about which zones of a mesh have the biggest influence over the point wise error in stresses at those points. This information indicates how to control that error in the most effective way by refining the mesh only at those zones.

Duality techniques have already been applied in order to get element bounds for functional outputs of different partial differential equations and the corresponding goal-oriented adaptive remeshing strategies (see Refs. [6–9]). The work presented here also provides a goal-oriented adaptive remeshing strategy based on a sensitivity analysis instead of the duality techniques.

The objective of the sensitivity analysis of a point wise error estimator is to know its derivative with respect to each of the nodal coordinates. This information provides a first order prediction of the variation of the point wise error estimator produced by a modification of the position of the nodal points. In this way, for a mesh with N nodal points the sensitivity analysis of a point wise error ''e'' provides the next vector of derivatives:

$$\frac{\mathrm{d}e}{\mathrm{d}\mathbf{x}} = \left[\frac{\mathrm{d}e}{\mathrm{d}x_1} \quad \frac{\mathrm{d}e}{\mathrm{d}y_1} \quad \frac{\mathrm{d}e}{\mathrm{d}x_2} \quad \frac{\mathrm{d}e}{\mathrm{d}y_2} \quad \cdots \quad \frac{\mathrm{d}e}{\mathrm{d}x_N} \quad \frac{\mathrm{d}e}{\mathrm{d}y_N} \right]^{\mathrm{T}}. \tag{1}$$

In this way, the first order prediction of the variation of the error that would be produced by an increment Δx_i of each nodal coordinate x_i would be:

$$\Delta e = \sum_{i=1}^{2N} \frac{\mathrm{d}e}{\mathrm{d}x_i} \Delta x_i = \frac{\mathrm{d}e}{\mathrm{d}\mathbf{x}} \Delta \mathbf{x}^{\mathrm{T}}. \tag{2}$$

In this work, the error e in expressions (1) and (2) corresponds with the estimated point wise error in the Von Mises stress $e^{\mathrm{Von\ Mises}}$. This estimation is based on the difference between the finite element stresses and the smoothed stresses obtained from the SPR procedure. The corresponding expression for this point wise error estimator is the following (see Bugeda [3] for more details):

$$e^{\mathrm{Von\ Mises}} = \sqrt{\frac{(\sigma_1^* - \sigma_2^*)^2 + (\sigma_2^* - \sigma_3^*)^2 + (\sigma_3^* - \sigma_1^*)^2}{6}} - \sqrt{\frac{(\hat{\sigma}_1 - \hat{\sigma}_2)^2 + (\hat{\sigma}_2 - \hat{\sigma}_3)^2 + (\hat{\sigma}_3 - \hat{\sigma}_1)^2}{6}}. \tag{3}$$

In expression (3), $\hat{\sigma}_i$ are the different principal components of the stress tensor obtained from the finite element analysis and σ_i^* are the corresponding values obtained from the SPR procedure.

This paper presents how the sensitivity analysis of the point wise error estimator can be computed and some of its possible applications including a new adaptive remeshing scheme.

2. Finite element approximation

Before to proceed to the sensitivity analysis it is convenient to review some aspects of the formulation of the equilibrium problem and the corresponding finite element discretisation. The equilibrium equations can be written as

$$\mathbf{L}\mathbf{u} - \mathbf{q} = \mathbf{0}. \tag{4}$$

Last equation is defined in the interior of a domain Ω where $\mathbf{u}$ is the displacements field, $\mathbf{L}$ is a second order linear operator and $\mathbf{q}$ is the volumetric force vector field. Eq. (4) is also complemented with the corresponding Dirichlet and Neumann boundary conditions.

During the finite element discretisation process we use the following approximation:

$$\mathbf{u} \approx \hat{\mathbf{u}} = \mathbf{N}\mathbf{a}, \tag{5}$$

where $\mathbf{N}$ contains the shape functions and $\mathbf{a}$ is the vector containing the nodal displacements. The Principle of Virtual Work drives us to the well known discrete equations:

$$\mathbf{K}\mathbf{a} = \mathbf{f}, \tag{6}$$

where

$$\mathbf{K} = \sum_{e=1}^{n^0 \text{elements}} \mathbf{K}_e \qquad \mathbf{K}_e = \int_{\Omega_e} \mathbf{B}^{\mathrm{T}}\mathbf{D}\mathbf{B}\, d\Omega = \int_{\Omega_\xi} \mathbf{B}^{\mathrm{T}}\mathbf{D}\mathbf{B}|\mathbf{J}|\, d\xi_1\, d\xi_2, \tag{7}$$

$$\mathbf{f} = \sum_{e=1}^{n^0 \text{elements}} \mathbf{f}_{\Omega_e} + \mathbf{f}_{\Gamma_e} \begin{cases} \mathbf{f}_{\Omega_e} = \int_{\Omega_e} \mathbf{N}^{\mathrm{T}}\mathbf{v}\, d\Omega = \int_{\Omega_\xi} \mathbf{N}^{\mathrm{T}}\mathbf{v}|\mathbf{J}|\, d\xi_1\, d\xi_2, \\ \mathbf{f}_{\Gamma_e} = \int_{\Gamma_e} \mathbf{N}^{\mathrm{T}}\mathbf{t}\, d\Gamma = \int_{\Gamma_\xi} \mathbf{N}^{\mathrm{T}}\mathbf{t}|\mathbf{J}|\, d\xi_1. \end{cases} \tag{8}$$

Being $\mathbf{f}_\Omega$ the vector due to the volumetric forces $\mathbf{v}$ and $\mathbf{f}_\Gamma$ the vector due to the surface forces $\mathbf{t}$. $|\mathbf{J}|$ is the determinant of the jacobian matrix of the transformation between the physical and the isoparametric domain for each of the elements whereas ξ_1 and ξ_2 are the corresponding isoparametric coordinates for a two dimensional case.

Obviously, the solution $\hat{\mathbf{u}}$ obtained from the Finite Element Method (FEM) is not the exact solution of (4) and the substitution of $\mathbf{u}$ by $\hat{\mathbf{u}}$ in the original equilibrium equations produces:

$$\mathbf{L}\hat{\mathbf{u}} - \mathbf{q} = \mathbf{r}_\Omega, \tag{9}$$

where $\mathbf{r}_\Omega$ is the residual or lack of equilibrium at each point. Most of the existing methods for the error estimation and its correction try to control the values and the distribution of the residual.

The relation between the nodal displacements $\mathbf{a}$ and the corresponding stresses and strains is the following:

$$\hat{\boldsymbol{\varepsilon}} = \mathbf{B}\mathbf{a}, \quad \hat{\boldsymbol{\sigma}} = \mathbf{D}\hat{\boldsymbol{\varepsilon}}, \tag{10}$$

where the matrix $\mathbf{B}$ contains the derivatives of the shape functions with respect to x and y, whereas the matrix $\mathbf{D}$ contains the elastic parameters of the material.

3. The "Superconvergent Patch Recovery" (SPR) technique

This section is dedicated to remind the different expressions related with the SPR method (see Zienkiewicz and Zhu [10]) that will be differentiated later. In this process, the smoothed stresses corresponding to a fixed nodal point are obtained from a polynomial expansion defined over a patch of elements centred

Triangular linear elements   Triangular quadratic elements
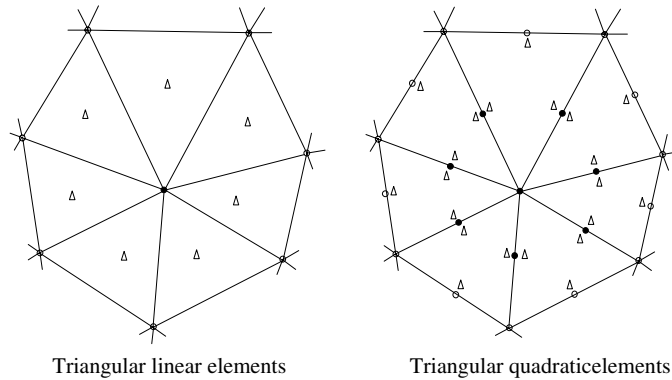
Fig. 1. Definition of the patches and the points for the evaluation of stresses.

on that node (see Fig. 1). This polynomial expansion is determined from a minimum square adjustment using the FEM values evaluated at the "superconvergent" points.

At each node, each of the stress components σ_i^* is obtained from a complete polynomial σ_{pi}^* whose degree p is the same used for the shape functions **N**. For each of the stress components of a plane stress situation $(\sigma_x, \sigma_y, \tau_{xy})$ this polynomial has the following expression:

$$\sigma_{pi}^* = \mathbf{p}\mathbf{b}, \tag{11}$$

where **p** contains the polynomial terms and **b** contains the polynomial coefficients. On the other hand, σ_{pi}^* corresponds with the i component of stress obtained in the patch. For the two dimensional linear case $\mathbf{p} = \{1, x, y\}$ and $\mathbf{b} = \{b_1, b_2, b_3\}^{\mathrm{T}}$ whereas for the two dimensional quadratic case $\mathbf{p} = \{1, x, y, x^2, xy, y^2\}$ and $\mathbf{b} = \{b_1, b_2, b_3, b_4, b_5, b_6\}^{\mathrm{T}}$.

The components of the **b** vector associated with each of the stress components are obtained by minimising the following residual:

$$R_{Gi}(\mathbf{b}) = \sum_{j=1}^{G} \left(\hat{\sigma}_i(\mathbf{x}_j) - \sigma_{pi}^* \right)^2 = \sum_{j=1}^{G} \left(\hat{\sigma}_i(\mathbf{x}_j) - \mathbf{p}(\mathbf{x}_j)\mathbf{b} \right)^2, \tag{12}$$

where $\mathbf{x}_j$ are the coordinates (x_j, y_j) of each of the points where the FEM stress components $(\hat{\sigma}_i)$ are evaluated, and $G = mk$ is the total number of those points, being k the number of those points at each of the m elements contained in the patch.

The minimisation of (12) produces the following expression:

$$\sum_{j=1}^{G} \mathbf{p}^{\mathrm{T}}(x_j, y_j)\mathbf{p}(x_j, y_j)\mathbf{b} = \sum_{j=1}^{G} \mathbf{p}^{\mathrm{T}}(x_j, y_j)\hat{\sigma}_i(x_j, y_j). \tag{13}$$

Last equation has to be solved for each of the stress components. This can be solved as

$$\mathbf{b} = \mathbf{A}^{-1}\mathbf{c} \quad \text{with} \quad \mathbf{A} = \sum_{j=1}^{G} \mathbf{p}^{\mathrm{T}}(x_j, y_j)\mathbf{p}(x_j, y_j) \quad \text{and} \quad \mathbf{c} = \sum_{j=1}^{G} \mathbf{p}^{\mathrm{T}}(x_j, y_j)\hat{\sigma}_j(x_j, y_j). \tag{14}$$

The number of equations to be solved at each patch is equal to the number of stress components multiplied by the number of components of the **b** vector (3 or 6). Matrix **A** is the same for all stress components and, for each patch, it only needs to be built and factorised once. This makes the computational cost of the SPR procedure very small compared with the cost of the FEM analysis.

Once the components of the vector **b** have been evaluated, the values of each of the components of the stress $\boldsymbol{\sigma}^*$ at any point can be evaluated by substituting its coordinates in expression (11).

The original SPR procedure that has been described here has been complemented by Wiberg et al. [11] for improving the accomplishment of the equilibrium equations and the boundary conditions applied to the smoothed stresses. Labbé and Garon [12] have also improved the robustness of the method at the boundary points.

In this work we have used the original version of the SPR method (see [10]).

4. Sensitivity analysis of the point wise estimations of the error

This section is devoted to the formulation of the sensitivity analysis of the point wise error estimator $e^{\text{Von Mises}}$, defined in expression (3), with respect to the mesh nodal coordinates.

4.1. Formulation of the adjoint-state

The error $e^{\text{Von Mises}}$ depends of the nodal displacements vector **a** and the nodal coordinates vector **x**. On the other hand, the displacements and the coordinates are related by the discrete equilibrium equations (6). For this reason, we can write the problem as the computation of the derivatives of $e^{\text{Von Mises}}$:

$$e^{\text{Von Mises}} = e^{\text{Von Mises}}(\mathbf{a}, \mathbf{x}), \tag{15}$$

where the fields **a** and **x** are related by the discrete equilibrium equations

$$\boldsymbol{\Psi} = \mathbf{K}(\mathbf{x})\mathbf{a} - \mathbf{f}(\mathbf{x}) = \mathbf{0}. \tag{16}$$

The lagrangian of $e^{\text{Von Mises}}$ under the restrictions (16) can be written as

$$L = e^{\text{Von Mises}} + \boldsymbol{\lambda}^{\text{T}}\boldsymbol{\Psi}, \tag{17}$$

where $\boldsymbol{\lambda}$ is a *n*-dimensional vector containing the Lagrange multipliers, typically named as the adjoint-state (see [13]). The derivatives of L with respect to **x** will be identical to the derivatives of $e^{\text{Von Mises}}$ because the vector $\boldsymbol{\Psi}$ must be identically zero. These derivatives can be computed as

$$\frac{\mathrm{d}L}{\mathrm{d}\mathbf{x}} = \frac{\mathrm{d}e^{\text{Von Mises}}}{\mathrm{d}\mathbf{x}} = \frac{\partial e^{\text{Von Mises}}}{\partial \mathbf{x}} + \frac{\partial e^{\text{Von Mises}}}{\partial \mathbf{a}}\frac{\partial \mathbf{a}}{\partial \mathbf{x}} + \boldsymbol{\lambda}^{\text{T}}\left(\frac{\partial \boldsymbol{\Psi}}{\partial \mathbf{x}} + \frac{\partial \boldsymbol{\Psi}}{\partial \mathbf{a}}\frac{\partial \mathbf{a}}{\partial \mathbf{x}}\right), \tag{18}$$

where the derivatives of $\boldsymbol{\lambda}$ have been omitted because they would be multiplied by $\boldsymbol{\Psi}$ that is identically null. The adjoint-state is selected as the solution of the following system of equations:

$$\frac{\partial e^{\text{Von Mises}}}{\partial \mathbf{a}} + \boldsymbol{\lambda}^{\text{T}}\frac{\partial \boldsymbol{\Psi}}{\partial \mathbf{a}} = \mathbf{0}. \tag{19}$$

This simplifies expression (18) now becoming:

$$\frac{\mathrm{d}e^{\text{Von Mises}}}{\mathrm{d}\mathbf{x}} = \frac{\partial e^{\text{Von Mises}}}{\partial \mathbf{x}} + \boldsymbol{\lambda}^{\text{T}}\frac{\partial \boldsymbol{\Psi}}{\partial \mathbf{x}}. \tag{20}$$

The main characteristic of the exposed method is that once all expressions have been evaluated the only system of equations that must be solved is (19). In addition, looking at (16) we can see that the matrix of this system is the same stiffness matrix of the FEM that has already been assembled and solved.

In the case of most goal oriented methods a system of equations similar to (19) is also solved where the independent term is the derivative of the goal magnitude with respect to the nodal displacements vector **a** (see Refs. [6–9]).

The obtainment of the partial derivatives of $e^{\text{Von Mises}}$ with respect to the vectors $\mathbf{a}$ and $\mathbf{x}$ appearing in (19) and (20) will be seen later. On the other hand, the computation of the partial derivative of $\mathbf{\Psi}$ with respect to the vector $\mathbf{a}$ is trivial looking at (16):

$$\frac{\partial \mathbf{\Psi}}{\partial \mathbf{a}} = \mathbf{K}. \tag{21}$$

Looking at (16) we can also see that the partial derivative of $\mathbf{\Psi}$ with respect to $\mathbf{x}$ appearing at (20) requires the computation of the partial derivatives of the stiffness matrix $\mathbf{K}$ and the nodal forces vector $\mathbf{f}$ with respect to the vector of nodal coordinates:

$$\frac{\partial \mathbf{\Psi}}{\partial \mathbf{x}} = \frac{\partial \mathbf{K}}{\partial \mathbf{x}} \mathbf{a} - \frac{\partial \mathbf{f}}{\partial \mathbf{x}}. \tag{22}$$

This computation can be considered as belonging to the state of the art in the context of the structural optimisation and the corresponding sensitivity analysis and, due to that, it is not detailed here. The corresponding expressions can be seen in [14]. The computation of the partial derivatives of the stiffness matrix $\mathbf{K}$ with respect to $\mathbf{x}$ is made by assembling the derivatives of each of the elemental matrices $\mathbf{K}_e$. These derivatives are obtained by using the isoparametric transformation concept that allows to use the following expression for the two dimensional case:

$$\frac{\partial \mathbf{K}_e}{\partial \mathbf{x}} = \int_{\Omega_\xi} \left[\frac{\partial \mathbf{B}^{\mathrm{T}}}{\partial \mathbf{x}} \mathbf{D} \mathbf{B} |\mathbf{J}| + \mathbf{B}^{\mathrm{T}} \mathbf{D} \frac{\partial \mathbf{B}}{\partial \mathbf{x}} |\mathbf{J}| + \mathbf{B}^{\mathrm{T}} \mathbf{D} \mathbf{B} \frac{\partial |\mathbf{J}|}{\partial \mathbf{x}} \right] \mathrm{d}\xi_1 \, \mathrm{d}\xi_2. \tag{23}$$

Similar concepts allow to compute the partial derivatives of the nodal forces vector $\mathbf{f}$ with respect to $\mathbf{x}$.

4.2. Computation of the partial derivatives of the point wise error estimator

The partial derivatives of $e^{\text{Von Mises}}$ with respect to the vector $\mathbf{a}$ appearing in (19) can be expressed in terms of the principal components of the stress tensors $\hat{\boldsymbol{\sigma}}$ and $\boldsymbol{\sigma}^*$, and their partial derivatives with respect to $\mathbf{a}$ by derivation of expression (3):

$$\frac{\partial e^{\text{Von Mises}}}{\partial \mathbf{a}} = \frac{(\sigma_1^* - \sigma_2^*)\left(\dfrac{\partial \sigma_1^*}{\partial \mathbf{a}} - \dfrac{\partial \sigma_2^*}{\partial \mathbf{a}}\right) + (\sigma_2^* - \sigma_3^*)\left(\dfrac{\partial \sigma_1^*}{\partial \mathbf{a}} - \dfrac{\partial \sigma_2^*}{\partial \mathbf{a}}\right) + (\sigma_3^* - \sigma_1^*)\left(\dfrac{\partial \sigma_1^*}{\partial \mathbf{a}} - \dfrac{\partial \sigma_2^*}{\partial \mathbf{a}}\right)}{6\sqrt{\dfrac{(\sigma_1^* - \sigma_2^*)^2 + (\sigma_2^* - \sigma_3^*)^2 + (\sigma_3^* - \sigma_1^*)^2}{6}}}$$
$$- \frac{(\hat{\sigma}_1 - \hat{\sigma}_2)\left(\dfrac{\partial \hat{\sigma}_1}{\partial \mathbf{a}} - \dfrac{\partial \hat{\sigma}_2}{\partial \mathbf{a}}\right) + (\hat{\sigma}_2 - \hat{\sigma}_3)\left(\dfrac{\partial \hat{\sigma}_1}{\partial \mathbf{a}} - \dfrac{\partial \hat{\sigma}_2}{\partial \mathbf{a}}\right) + (\hat{\sigma}_3 - \hat{\sigma}_1)\left(\dfrac{\partial \hat{\sigma}_1}{\partial \mathbf{a}} - \dfrac{\partial \hat{\sigma}_2}{\partial \mathbf{a}}\right)}{6\sqrt{\dfrac{(\hat{\sigma}_1 - \hat{\sigma}_2)^2 + (\hat{\sigma}_2 - \hat{\sigma}_3)^2 + (\hat{\sigma}_3 - \hat{\sigma}_1)^2}{6}}}. \tag{24}$$

The partial derivatives of the principal components of the stress tensors $\hat{\boldsymbol{\sigma}}$ and $\boldsymbol{\sigma}^*$ with respect to the nodal displacements vector $\mathbf{a}$ can be expressed in terms of their cartesian stress components and the corresponding partial derivatives by derivation of the explicit expression that provides the principal stresses in terms of the stress components. For instance, for the two-dimensional case we have that the two principal components of any stress tensor $\boldsymbol{\sigma}$ can be written as

$$\sigma_{1,2} = \frac{\sigma_x + \sigma_y}{2} \pm \sqrt{\left(\frac{\sigma_x - \sigma_y}{2}\right)^2 + \tau_{xy}^2}. \tag{25}$$

Then, their corresponding partial derivatives with respect to the mesh nodal coordinates are:

$$\frac{\partial \sigma_{1,2}}{\partial \mathbf{a}} = \frac{1}{2}\left(\frac{\partial \sigma_x}{\partial \mathbf{a}} + \frac{\partial \sigma_y}{\partial \mathbf{a}}\right) \pm \frac{\left(\frac{\sigma_x - \sigma_y}{2}\right)\left(\frac{\partial \sigma_x}{\partial \mathbf{a}} - \frac{\partial \sigma_y}{\partial \mathbf{a}}\right) + 2\tau_{xy}\frac{\partial \tau_{xy}}{\partial \mathbf{a}}}{2\sqrt{\left(\frac{\sigma_x - \sigma_y}{2}\right)^2 + \tau_{xy}^2}}.$$

(26)

Expressions (25) and (26) can be used for the obtainment of the partial derivatives of the principal components of any of the stress tensors $\hat{\boldsymbol{\sigma}}$ and $\boldsymbol{\sigma}^*$ in terms of the partial derivatives of their respective cartesian stress components. In addition, the same approach used in expressions (24)–(26) can also be used for the obtainment of the partial derivatives of $e^{\text{Von Mises}}$ with respect to the vector of nodal coordinates $\mathbf{x}$ appearing in (20). The corresponding expressions are identical to (24) and (26) with the only difference that the partial derivatives with respect to $\mathbf{a}$ are substituted by partial derivatives with respect to $\mathbf{x}$.

After the previous process, the reminding part of the sensitivity analysis of $e^{\text{Von Mises}}$ with respect to the vector of nodal coordinates is the computation of the partial derivatives of the cartesian components of $\hat{\boldsymbol{\sigma}}$ and $\boldsymbol{\sigma}^*$ with respect to the vectors $\mathbf{a}$ and $\mathbf{x}$. This is described in next subsections.

4.3. Computation of the partial derivative of the FEM stresses $\hat{\boldsymbol{\sigma}}$

For the computation of the partial derivatives of the values of the stress vector $\hat{\boldsymbol{\sigma}}$ obtained for a fixed point from the discrete equations we can just do the following:

$$\hat{\boldsymbol{\sigma}} = \mathbf{BDa}, \quad \frac{\partial \hat{\boldsymbol{\sigma}}}{\partial \mathbf{a}} = \mathbf{BD}, \quad \frac{\partial \hat{\boldsymbol{\sigma}}}{\partial \mathbf{x}} = \frac{\partial \mathbf{B}}{\partial \mathbf{x}}\mathbf{Da}.$$

(27)

The partial derivatives of $\mathbf{B}$ have already appeared in (23) and the corresponding formulation can be seen in [14].

4.4. Computation of the partial derivative of the SPR stresses $\boldsymbol{\sigma}^*$

Starting from (11) and (14), the computation of the partial derivatives of each of the stress components σ_{pi}^* with respect to the nodal displacements vector $\mathbf{a}$ can be obtained using the chain rule of derivation:

$$\frac{\partial \sigma_{pi}^*}{\partial \mathbf{a}} = \mathbf{p}\frac{\partial \mathbf{b}}{\partial \mathbf{a}} = \mathbf{pA}^{-1}\frac{\partial \mathbf{c}}{\partial \mathbf{a}},$$

(28)

$$\frac{\partial \mathbf{c}}{\partial \mathbf{a}} = \sum_{j=1}^{G} \mathbf{p}^{\mathrm{T}}(x_j, y_j)\frac{\partial \hat{\sigma}_j(x_j, y_j)}{\partial \mathbf{a}}.$$

(29)

In last expressions it has been taken into account that neither the expression of the matrix $\mathbf{A}$ nor the evaluation of the polynomials $\mathbf{p}$ are dependent of the displacements $\mathbf{a}$. On the other hand, the partial derivatives of the stress components $\hat{\sigma}_j(x_j, y_j)$ with respect to the displacements vector can be obtained from (27).

The derivatives of each of the stress components σ_{pi}^* with respect to the nodal coordinates vector $\mathbf{x}$ can be obtained from the following expression:

$$\frac{\partial \sigma_{pi}^*}{\partial \mathbf{x}} = \mathbf{p}\frac{\partial \mathbf{b}}{\partial \mathbf{x}}.$$

(30)

Starting from (27) and taking into account that $\mathbf{c} = \mathbf{Ab}$ we can do:

$$\frac{\partial \mathbf{c}}{\partial \mathbf{x}} = \frac{\partial \mathbf{A}}{\partial \mathbf{x}}\mathbf{b} + \mathbf{A}\frac{\partial \mathbf{b}}{\partial \mathbf{x}}, \quad \frac{\partial \mathbf{b}}{\partial \mathbf{x}} = \mathbf{A}^{-1}\left[\frac{\partial \mathbf{c}}{\partial \mathbf{x}} - \frac{\partial \mathbf{A}}{\partial \mathbf{x}}\mathbf{b}\right].$$

(31)

The new partial derivatives appearing in (31) can be obtained from the following expressions:

$$\frac{\partial \mathbf{c}}{\partial \mathbf{x}} = \sum_{j=1}^{G} \left[\frac{\partial \mathbf{p}^{\mathrm{T}}(x_j, y_j)}{\partial \mathbf{x}} \hat{\sigma}_j(x_j, y_j) + \mathbf{p}^{\mathrm{T}}(x_j, y_j) \frac{\partial \hat{\sigma}_j(x_j, y_j)}{\partial \mathbf{x}} \right], \tag{32}$$

$$\frac{\partial \mathbf{A}}{\partial \mathbf{x}} = \sum_{j=1}^{G} \left[\frac{\partial \mathbf{p}^{\mathrm{T}}(x_j, y_j)}{\partial \mathbf{x}} \mathbf{p}(x_j, y_j) + \mathbf{p}^{\mathrm{T}}(x_j, y_j) \frac{\partial \mathbf{p}(x_j, y_j)}{\partial \mathbf{x}} \right]. \tag{33}$$

The partial derivative of the term $\hat{\sigma}_j$ can be obtained from (27). The partial derivatives of each of the components of the polynomial vector $p_k(x_j, y_j)$ evaluated at the point (x_j, y_j) can be obtained from:

$$\frac{\partial p_k(x_j, y_j)}{\partial \mathbf{x}} = \frac{\partial p_k(x_j, y_j)}{\partial x_j} \frac{\partial x_j}{\partial \mathbf{x}} + \frac{\partial p_k(x_j, y_j)}{\partial y_j} \frac{\partial y_j}{\partial \mathbf{x}}. \tag{34}$$

Due to the polynomial expression of each of the components p_k its differentiation with respect to any of the coordinates (x_j, y_j) is trivial. On the other hand, the differentiation of these coordinates with respect to the nodal coordinates $\mathbf{x}$ will have no null values only if we are differentiating with respect to a nodal point whose position affects to the position of point (x_j, y_j).

5. Application examples

This section shows two examples of use of the presented sensitivity analysis of the point wise error estimators.

5.1. Circular ring with an interior load

This first example is the analysis of a circular ring with an interior distributed load that can be seen in Fig. 2. The objectives of this example are:

- The analysis of the possibilities of the presented sensibility analysis for predicting the new values of the point wise error estimators when the finite element mesh is perturbed by modifying its nodal coordinates.
- The development of a new adaptive remeshing scheme based on the presented sensitivity analysis.
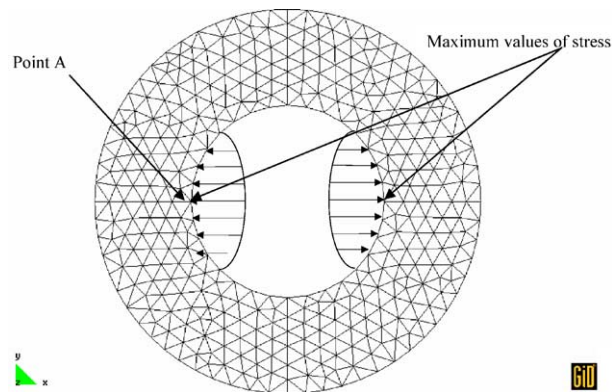

Fig. 2. Triangular quadratic finite element mesh with 666 elements and 1428 nodal points.

Fig. 2 also shows the finite element mesh used for this analysis with triangular quadrilateral elements. The internal radius of the geometry is 10 m whereas the external one is 20 m. The structural analysis has been made with a Young modulus $E = 3.1 \times 10^4$ MPa and a Poisson ratio $\gamma = 0.25$. The maximum value of the distributed load is 1.0 N/m^2.

The points where the highest values of stress appear are shown in Fig. 2. The exact value of the equivalent Von Mises stress at those points, obtained with an extremely fine mesh, is $\sigma^{\text{Von Mises}} = 2.15$ Pa.

Fig. 3 show the distribution of the Von Mises stress.

The values of the Von Mises stress at point A have been computed in two different ways:

- Directly from the finite element solution as the average of the stress values at point A obtained at all the elements containing that point.
- From the values provided at point A by the SPR method.

The estimation of the point wise error in the Von Mises equivalent stress at point A have been computed using expression (3) and have been compared with the exact point wise error. The corresponding comparison can be seen in Table 1.

Table 1 shows how the SPR values represent an improvement with respect to the FEM values but this improvement is not enough to ensure a good quality of the point wise error estimation which is very underestimated. It is well known that the stress recovery processes produce the worst predictions when applied to boundary points (see [11,12]). The percentage of error in the energy norm corresponding to this mesh is smaller than a 4%.

Fig. 4 shows the scalar distribution of the modules of the two components of the sensitivity analysis corresponding to each nodal point. Fig. 5 shows a representation where, at each nodal point, the vector represents the two components of the sensitivity analysis.
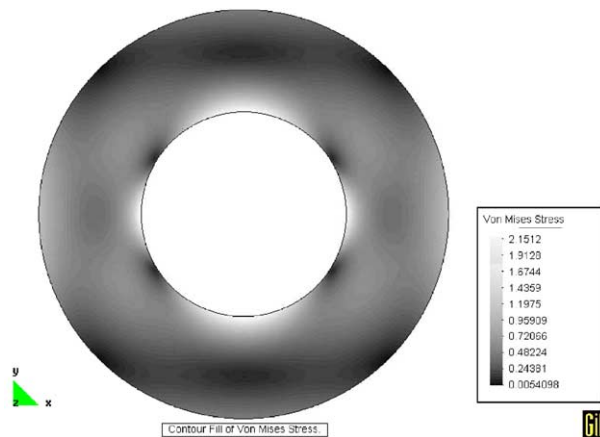

Fig. 3. Distribution of the Von Mises stress.

Table 1
Values of stress and estimated and real point wise errors at point A

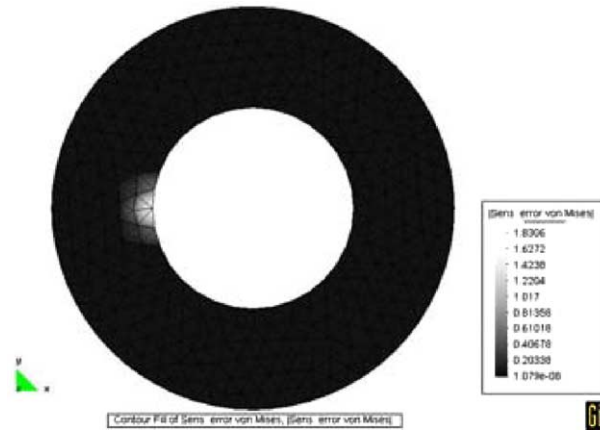|	FEM values	SPR values	Exact values	Estimated error	Exact error
$\sigma^{\text{Von Mises}}$	1.91	1.96	2.15	0.05	0.24

All the values are in Pa.

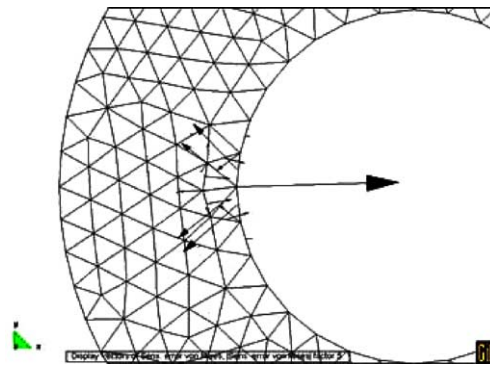Fig. 4. Scalar representation of the sensitivity analysis of the error in the Von Mises stress.

Fig. 5. Vector representation of the sensitivity analysis of the error in the Von Mises stress.

Figs. 4 and 5 show that the represented sensitivity analysis presents relevant values only at the vicinity of point A. This suggests that the first order approximation of the point wise error at point A only depends on the coordinates of the nodes located close to it. This also suggests that, in this case, there is not any presence of pollution error coming far from point A. In fact, this is the expected behaviour of the error due to the fact that this problem does not present any source of pollution error like a singular point or a point with a relevant concentration of stresses.

5.1.1. Quality of the presented formulation for the sensitivity analysis

In order to check the quality of the presented sensitivity analysis we have proceeded to perturbate the mesh and to compare the prediction of the point wise error estimation obtained by using expression (2) with the values computed using the new mesh. The perturbation of the mesh has been done by displacing each node in the direction of the considered sensitivity analysis and in the opposite sense. This is, in fact, the perturbation that should produce the quickest first order minimisation of the values of the point wise error estimations. The vector containing the nodal coordinates has been incremented using the following expression:

$$\Delta \mathbf{x} = -\kappa \frac{\mathrm{d}e^{\mathrm{Von\,Mises}}}{\mathrm{d}\mathbf{x}} \tag{35}$$

where κ is a factor that controls the size of the mesh perturbation. In order to avoid a possible modification of the boundary shape during the perturbation due to the movement of the boundary nodes, the sensitivity vector at those nodes has been projected over the tangent direction to the boundary. The value of κ has been progressively increased and, for each value, the following quantities have been computed:

- The value of the point wise estimation of the maximum error in stress at point A computed from a new analysis for each value of κ.
- An estimation of this value using the information obtained with the initial mesh and the corresponding sensitivity analysis. In this case, for each value of κ the increment of the estimation of the point wise error has been obtained with:

$$\Delta e^{\text{Von Mises}} = \kappa \left(\frac{d e^{\text{Von Mises}}}{d\mathbf{x}} \right)^2. \tag{36}$$

Fig. 6 shows the described comparisons. It can be seen how for values of κ smaller than 0.02 the agreement between the computed and the predicted values is practically perfect. For larger values of κ the first order prediction provided by the sensitivity analysis is not enough for a good prediction of the evolution of the error estimation. Good predictions for higher values of κ would require a higher order sensitivity analysis.

5.1.2. Minimisation of the point wise error estimation by moving the nodal points (r-adaptivity)

Another application of the sensitivity analysis is the minimization of the point wise error estimation in terms of the nodal coordinates. This is, in fact, an optimization problem where the objective function is the error measure to be minimized and the corresponding sensitivity analysis is the one presented in this work. The used minimisation algorithm is the following:
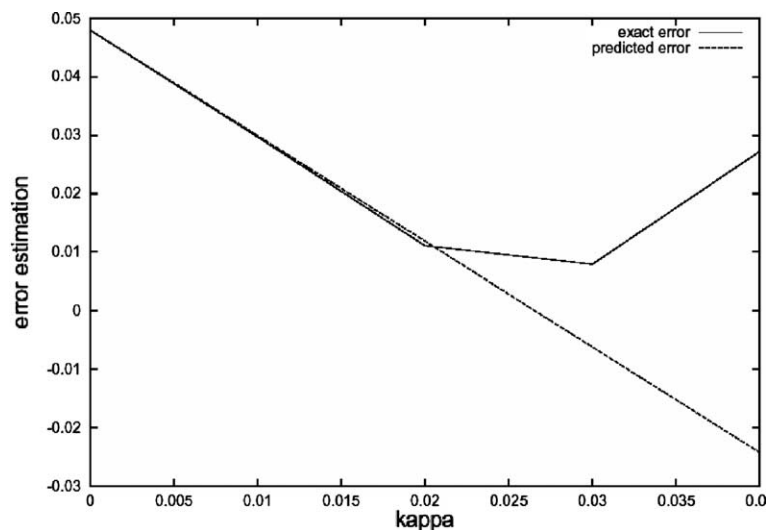

Fig. 6. Comparisons between the computed and the predicted point wise error estimations.

Table 2
New stress values after the minimization of the error

	Initial FEM	Initial SPR	Final FEM	Final SPR	Exact values	Improvement in FEM values	Improvement in SPR values
$\sigma^{\text{Von Mises}}$	1.91	1.96	2.03	2.03	2.15	0.12	0.07

All the values are in Pa.

1. For the minimisation of $e^{\text{Von Mises}}$ the nodal coordinates of the mesh are modified using expression (35) and the corresponding sensitivity analysis.
2. The optimum value of κ is chosen by performing a line search looking for the minimum value of the selected error.
3. The sensitivity analysis is computed again for the modified mesh and the process goes back to point 1.

The process stops when no more reductions of the estimated error are obtained or when the mesh becomes too much distorted.

Table 2 shows the final values of stresses obtained after the described error minimization process. This table allows to compare the new values of stress with the previous ones and with the exact ones.

The minimized error estimation has becomed null because after the modification of the mesh the FEM stresses and the SPR stresses have become identical. In fact, the mesh has been slightly distorted in order to produce SPR stresses identical to the FEM ones. It does not means that the exact error after the process be null. Anyway, the exact error in both the FEM stresses and the SPR stresses has been reduced. This reduction has been bigger for the FEM values. The modification of the nodal coordinates are very small and the modified meshes are practically identical to the original ones.

5.1.3. Adaptive remeshing scheme (h-adaptivity)

As stated in the introduction of this paper, when doing a structural analysis we know very often where the points with the highest values of stresses are. Nevertheless, when developing an adaptive remeshing scheme, the control of the pollution error obligates to control the point wise error not only at those points but everywhere, this producing very expensive meshes for just evaluating the stresses at those points (see [3] for more details). In order to overcome this situation we propose a new adaptive remeshing scheme based on the reduction of the element size only at the zones where the error sensitivity analysis produce relevant values, i.e., the zones where the corresponding nodal coordinates are relevant for the value of the error. In this way, at each nodal point i a new element size h_i^{new} is computed by reducing the old size h_i^{old} proportionally to the derivatives of the error with respect to the nodal coordinates x_i and y_i. The old size h_i^{old} can be computed as the mean size of the elements connected with the ith node. Each new value of h_i can be computed then as

$$h_i^{\text{new}} = h_i^{\text{old}} \left(1 - \mu \sqrt{\left(\frac{de^{\text{Von Mises}}}{dx_i}\right)^2 + \left(\frac{de^{\text{Von Mises}}}{dy_i}\right)^2} \right). \tag{37}$$

The value of μ is used to avoid negative values of the new element sizes by using:

$$\mu = \min \left(\frac{0.9 h_i^{\text{old}}}{\sqrt{\left(\frac{de^{\text{Von Mises}}}{dx_i}\right)^2 + \left(\frac{de^{\text{Von Mises}}}{dy_i}\right)^2}}, \quad \text{for } i = 1,\ldots, \text{total number of nodes} \right). \tag{38}$$

In the case of the circular ring example the highest values of stress are clearly located at point A. Thus, we have proceeded with the adaptive remeshing scheme presented in expressions (37) and (38). Fig. 7 shows the final mesh obtained after three adaptive remeshing loops that can be compared with the initial one. It
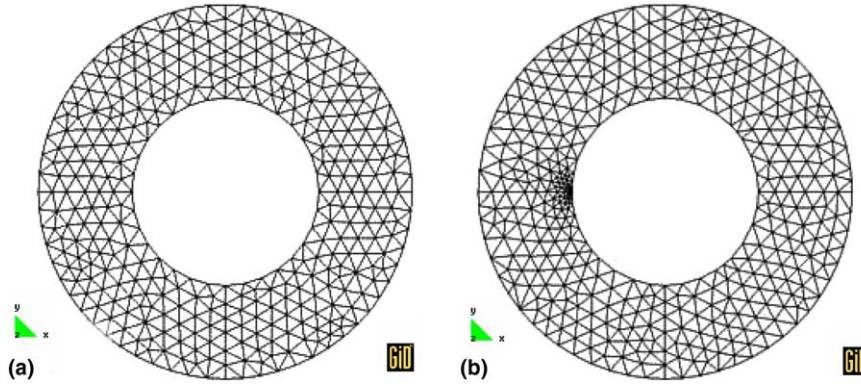
Fig. 7. (a) Initial mesh with 1428 nodal points and 666 elements. (b) Mesh obtained after the third remeshing step with 1680 nodal points and 786 elements.
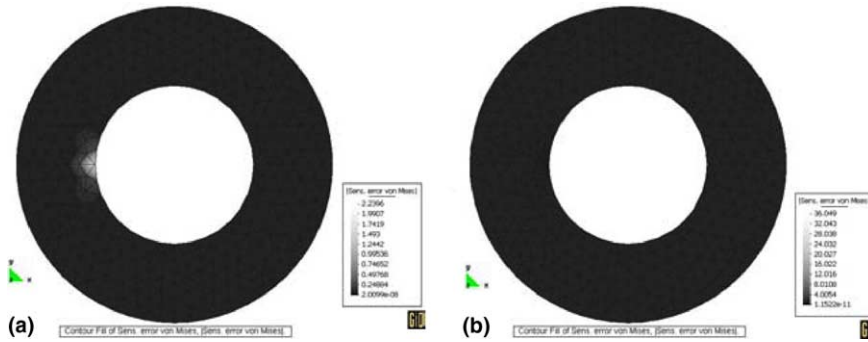

Fig. 8. (a) Sensitivity analysis of the error in the equivalent Von Mises stress for the initial mesh. (b) Sensitivity analysis of the error in the equivalent Von Mises stress after the three remeshing steps.

can be observed how the adapted mesh concentrates additional elements around point A whereas the rest of the domain remains practically unaltered. Fig. 8 shows the distribution of the sensitivity analysis of the estimated point wise error in the equivalent Von Mises stress with respect to the nodal coordinates. For the adapted mesh the non zero values of the sensitivity analysis are concentrated in a very reduced vicinity point A whereas in the rest of the domain it is practically null.

Table 3 shows the final values of stresses at point A obtained which each of the obtained meshes. It can be seen how the last mesh produces a prediction of the equivalent Von Mises stress at point A with three significant digits of precision. Different numerical experiments have shown that a globally adapted mesh using any standard adaptive remeshing procedure (see Ref. [3]) would require more than 20,000 nodal

Table 3
New stress values with each adapted mesh

	Initial mesh FEM	Initial mesh SPR	Second mesh FEM	Second mesh SPR	Third mesh FEM	Third mesh SPR	Fourth mesh FEM	Fourth mesh SPR	Exact values
$\sigma^{\text{Von Mises}}$	1.910	1.958	2.131	2.134	2.134	2.139	2.151	2.150	2.153

All the values are in Pa.

points and 9000 elements for producing a similar precision in the prediction of the Von Mises stress at point A, this being much more expensive than the mesh presented in Fig. 7b with only 1680 nodal points and 786 elements.

The adaptive remeshing scheme presented here does not provide any control neither over the final error at point A after the remeshing operations nor over the number of elements of the final mesh. Nevertheless, this last aspect could be easely obtained by multiplying expression (37) by a scalar factor and adjusting this factor in order to obtain a predefined number of elements. For triangular elements, this could be done as follows:

$$h_i^{\text{new}} = \omega h_i^{\text{old}} \left(1 - \mu \sqrt{\left(\frac{\mathrm{d}e^{\text{Von Mises}}}{\mathrm{d}x_i} \right)^2 + \left(\frac{\mathrm{d}e^{\text{Von Mises}}}{\mathrm{d}y_i} \right)^2} \right), \tag{39}$$

$$\omega = \frac{2}{N} \int_{\Omega} \frac{\mathrm{d}\Omega}{h^{\text{new}}}, \tag{40}$$

where N is the desired number of elements and h^{new} is a value that can be interpolated at each point from the nodal values given by (37). This technique could provide a possibility for densifying/coarsening meshes while maintaining a good level of precision at point A.

5.2. L shaped domain

This second example has been used to check the capability of the presented sensitivity analysis for detecting the presence of a significant amount of pollution error when estimating the point wise error in stresses at a specific point and to see the capabilities of the presented adaptive remeshing scheme in the presence of pollution error. The selected problem is the very well known L shaped domain shown in Fig. 9. This geometry presents a singular point at the interior corner that disseminates pollution error to the rest of the domain unless its surrounding zone be well discretised (see Refs. [4,5]).

The capability of the presented sensitivity analysis for detecting the pollution error has been tested by comparing the results obtained with different meshes with a different degree of discretisation. Fig. 9 shows the first of the employed meshes together with the position of the point where the point wise error estimations and the corresponding sensitivity analysis have been evaluated. This mesh has 202 triangular linear elements and 122 nodal points.

Fig. 10 shows the sensitivity analysis of the point wise estimation of the error in the Von Mises stress. As it can be seen, this sensitivity analysis presents significant values at zones located far away from the control
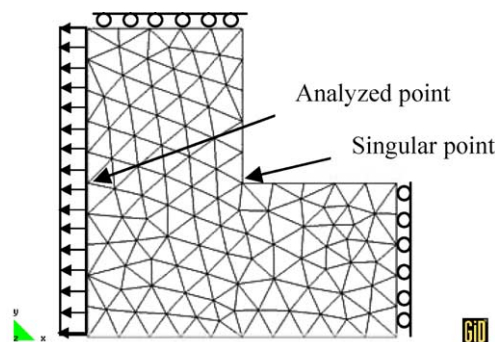

Fig. 9. Initial mesh, loads and boundary conditions for the L shaped domain problem.
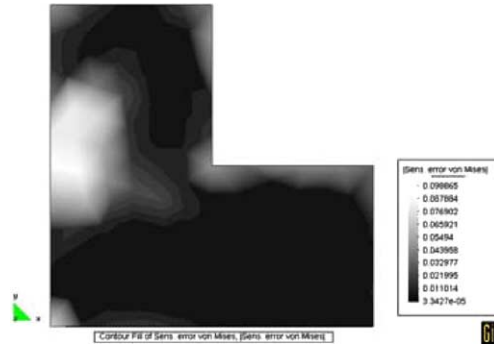
Fig. 10. Sensitivity analysis of the point wise estimation of the error in the Von Mises stress.

point and, in particular, in the zones located at the corner points like the singular one. This reflects that the magnitude of the estimated point wise error presents a clear dependence with respect to the quality of the mesh in zones located far away from the controlled point indicating the presence of pollution error. This behaviour is radically different to that of the previous example where there was not any singular point.This analysis has been repeated with the uniform mesh shown in Fig. 11. This new mesh has 2144 triangular linear elements and 1141 nodal points. Fig. 12 shows the corresponding sensitivity analysis with the new mesh. In this case, the relevant values of the sensitivity analysis only appear in the surrounding of the controlled point and not around the corner points. Only a very small zone around the singular point still presents non null values of these sensitivities. Experiments developed with even more dense meshes have sown that these small zones around the singularity disappear when improving the quality of the mesh. This demonstrates that the improvement of the mesh around the singular points diminishes the local error at that zones and the pollution error transferred to the rest of the domain as shown by Babuška et al. in Refs. [4,5].

The adaptive remeshing procedure described for the previous example has also been applied to the present one. Fig. 13 shows the comparison between the initial mesh and the mesh obtained after four remeshing steps. In this case, the remeshing procedure has concentrated a lot of elements around the controlled point but, in addition, it has also reduced the element size around the interior corner point. Fig. 14 shows how the new adapted mesh presents a uniform distribution of the error sensitivity analysis with the exception of a very small zone around the controlled point. This indicates the absence of pollution error in the adapted mesh.
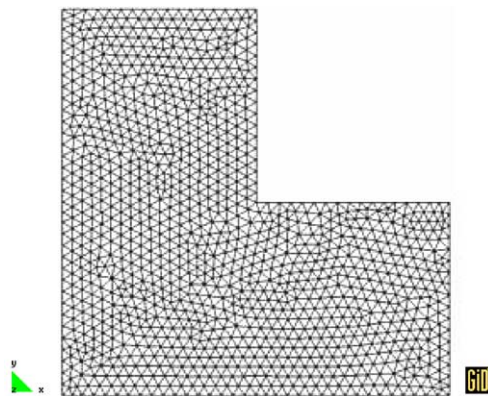

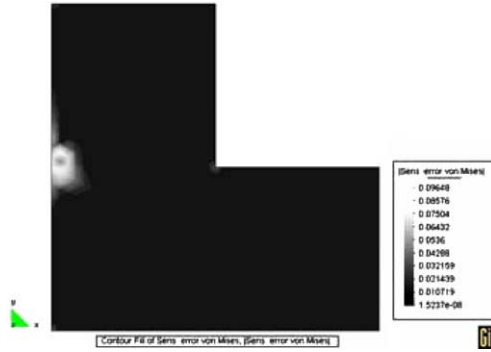Fig. 11. Second mesh for the L shaped domain.

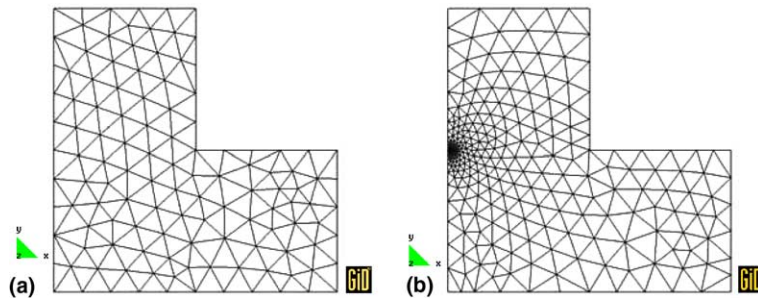Fig. 12. Sensitivity analysis of the point wise estimation of the error in the Von Mises stress.

Fig. 13. (a) Initial mesh with 122 nodal points and 202 elements. (b) Mesh obtained after the fourth remeshing step with 296 nodal points and 529 elements.
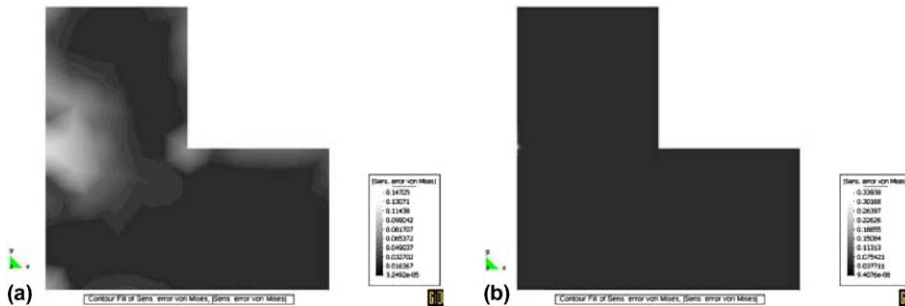

Fig. 14. (a) Sensitivity analysis of the error in the equivalent Von Mises stress for the initial mesh. (b) Sensitivity analysis of the error in the equivalent Von Mises stress after the four remeshing steps.

6. Conclusions

The main conclusions of this work can be summarized as follows:

- The sensitivity analysis of the point wise estimation of different measures of the error in stresses has been developed based on the adjoint state method.

- The sensitivity analysis is able to predict the changes in the error estimation produced by a perturbation of the mesh.
- The presented sensitivity analysis has also some capabilities for improving the point wise stress values by minimizing the point wise error estimation.
- The use of the presented sensitivity analysis for the detection of the pollution error due to a bad discretisation around singular or stress concentration points has also been checked.
- A new adaptive remeshing strategy based on the use of the sensitivity analysis of the point wise stress error estimation has been proposed. This new strategy produces very cheap meshes for the evaluation of accurate stresses at a specific point controlling also the amount of pollution error.

References

[1] B.M. McNeic, P.V. Marcal, Optimization of Finite Element Grids Based on Maximum Potential Energy, Technical Report no. 7, Brown University, Providence, 1971.

[2] Kang, K. Tae, B.M. Kwak, Optimization of finite element grids using shape sensitivity analysis in terms of nodal positions, Finite Elements Anal. Des. 26 (1997) 1–19.

[3] G. Bugeda, A comparison between new adaptive remeshing strategies based on point wise error estimation and energy norm error estimation, Commun. Numer. Methods Engrg. 18 (2002) 469–482.

[4] I. Babuška, T. Strouboulis, C.S. Upadhyay, S.K. Gangaraj, A posteriori estimation and adaptive control of the pollution error in the h-version of the finite element method, Int. J. Numer. Methods Engrg. 38 (1995) 4207–4235.

[5] I. Babuška, T. Strouboulis, S.K. Gangaraj, C.S. Upadhyay, Pollution error in the h-version of the finite element method and the local quality of the recovered derivatives, Comput. Methods Appl. Mech. Engrg. 140 (1997) 1–37.

[6] M. Paraschivoiu, J. Peraire, A. Patera, A posteriori finite element bounds for linear-functional outputs of elliptic partial differential equations, Comput. Methods Appl. Mech. Engrg. 150 (1997) 289–312.

[7] F. Cirak, E. Ramm, A posteriori error estimation and adaptivity for linear elasticity using the reciprocal theorem, Comput. Methods Appl. Mech. Engrg. 156 (1998) 351–362.

[8] J.T. Oden, S. Prudhomme, Goal-oriented error estimation and adaptivity for the finite element method, Comput. Math. Appl. 41 (2001) 735–756.

[9] A. Huerta, N. Parés, P. Díez, Flux free residual a posteriori error estimators yielding simultaneous upper and lower bounds of the error, in: N.E. Wiberg, P. Díez (Eds.), Proceedings of the Adaptive Modeling and Simulation Congress (ADMOS), CIMNE, Goteborg, 2003.

[10] O.C. Zienkiewicz, J.Z. Zhu, Superconvergence derivative recovery techniques and a posteriori error estimation in the finite element method. Part I and Part II, Int. J. Numer. Methods Engrg. 33 (1992) 1331–1382.

[11] N.E. Wiberg, F. Abdulwahab, S. Ziukas, Enhanced superconvergent patch recovery incorporating equilibrium and boundary conditions, Int. J. Numer. Methods Engrg. 37 (1994) 3417–3440.

[12] P. Labbé, A. Garon, A robust implementation of Zienkiewicz and Zhu's local patch recovery method, Comm. Appl. Numer. Methods 11 (1995) 427–434.

[13] G.A. Galarza, J. Carrera, A. Medina, Computational techniques for optimization of problems involving non-linear transient simulations, Int. J. Numer. Methods Engrg. 45 (1999) 319–334.

[14] F. Navarrina, E. Bendito, M. Casteleiro, High-order sensitivity analysis in shape optimization problems, Comput. Methods Appl. Mech. Engrg. 75 (1989) 267–281.